Table IV. Scalar Phosphorus-Copper Coupling Constants, a/h, and Bond Lengths, r(Cu-P), for a Number of (Triarylphosphine)copper(I) Halide Complexes[a]

compound	Cu coord no.	(a/h)/kHz	r(Cu-P)/Å	R^b
$[P(2,4,6)_3CuCl]$	2	2.04	2.18	0.61
$[P(2,4,6)_3CuBr]$	2	2.03	2.20	0.59
$[PPh_3CuCl]_4$	4	1.95	2.19	0.63
$[PPh_3CuBr]_4$	4	1.88	2.21	0.63
$[(PPh_3)_2CuCl]\cdot 0.5C_6H_6$	3	1.21	2.27	0.91
$[(PPh_3)_2CuBr]\cdot 0.5C_6H_6$	3	1.20	2.27	0.92
$[(PPh_3)_3CuCl]$	4	0.93	2.35	1.07
$[(PPh_3)_3CuBr]$	4	0.93	2.35	1.07

[a] ^{31}P solid-state NMR and structural data from this work and ref 2, 3, 16, and 17. [b] R is the ratio of the Cu-P dipolar coupling constant to the Cu-P scalar coupling constant (eq 2).

latter case is closer to tetrahedral, where the copper quadrupole coupling constant would be zero. Also, for both sets of compounds, the coupling constant for the chloro compound is greater than that for the bromo compound. This is consistent with the previously observed trend for the CuX and $[CuX_2]^-$ species, which has been attributed to a greater contraction of the Cu $4p_z$ orbital in the chloro complex relative to the bromo complex.[19,20] In the L_nCuX complexes there is the additional factor that CuCl is expected to be a stronger electron acceptor than CuBr, so the population of the Cu $4p_z$ orbital is likely to be greater in the CuCl complexes, resulting in a greater copper quadrupole coupling constant.

The scalar phosphorus-copper coupling constants a/h determined by the above procedure are in all cases almost exactly equal to the mean of the three line spacings. From the data used to construct Figure 5, it can be shown that this is true to within an error of less than 1% for $0 < K < 0.2$. The scalar coupling constants obtained for $[P(2,4,6)_3CuX]$ and for a number of related compounds with different copper coordination numbers are given in Table IV. It is clear that there is no direct correlation of these coupling constants with the copper coordination number. There is, however, a reasonable correlation with the Cu-P bondlengths, the coupling constant decreasing with increasing bond length. The dipolar coupling constant is proportional to the inverse cube of the bond length, so this also decreases with increasing bond length. However, the rates of decrease of the two coupling constants with increasing r(Cu-P) are not the same, so that the ratio R of the dipolar to the scalar coupling (eq 1) increases with increasing r(Cu-P) (Table IV). This suggests that further progress in the determination of copper quadrupole coupling constants from phosphorus-copper splitting patterns may require that calculations be carried out for a range of R values above 0.5, the value used in the only available published analysis.[15] We are currently carrying out such calculations.

Acknowledgment. We acknowledge support of this work by a grant from the Australian Research Grants Scheme and the New Zealand University Grants Committee. The Bruker CXP-300 spectrometer is operated by the Brisbane NMR Centre, and we thank the Centre for making instrument time available to us and to Dr. Peter Barron for recording the solid-state spectra. Microanalyses were completed by the University of Queensland Microanalytical Service.

Registry No. $[P(2,4,6)_3CuCl]$, 119638-24-3; $[P(2,4,6)_3CuBr]$, 119176-00-0.

Supplementary Material Available: Tables Sup I-Sup IV, listing non-hydrogen thermal parameters, the derived hydrogen positions, ligand non-hydrogen geometries, and crystal data (6 pages); tables of calculated and observed structure factors (16 pages). Ordering information is given on any current masthead page.

---

(19) Bowmaker, G. A.; Boyd, P. D. W. *J. Mol. Struct.* (*THEOCHEM*) **1985**, *122*, 299.

(20) Bowmaker, G. A.; Boyd, P. D. W.; Sorrenson, R. J. *J. Chem. Soc., Faraday Trans. 2* **1985**, *81*, 1627.

Contribution from the Laboratoire de Chimie Théorique, Bâtiment 490, Université de Paris-Sud, 91405 Orsay, France,
Department of Chemistry, North Carolina State University, Raleigh, North Carolina 27695-8204,
and Laboratoire d'Etudes des Propriétés Electroniques des Solides, CNRS, B.P. 166, 38042 Grenoble, France

Band Electronic Structure Study of the Electronic Instability in the Magnéli Phase Mo_4O_{11}

Enric Canadell,*[1a] Myung-Hwan Whangbo,*[1b] Claire Schlenker,[1c] and Claude Escribe-Filippini[1c]

Received September 29, 1988

To probe the origin of the resistivity anomaly in the Magnéli phases γ- and η-Mo_4O_{11}, we carried out tight-binding band electronic structure calculations on their common building block, the Mo_6O_{22} layer made up of MoO_6 octahedra. With two d electrons per formula unit Mo_4O_{11}, the bottom three bands of the Mo_6O_{22} layer are partially filled. The Fermi surfaces of those partially filled bands are all closed, in agreement with the observation that Mo_4O_{11} is a two-dimensional metal. Nevertheless, the Fermi surfaces have a partial nesting consistent with the superlattice spots at (0, 0.23b^*, 0) observed for η-Mo_4O_{11}. A charge density wave associated with this partial nesting is most likely to cause the resistivity anomaly in γ- and η-Mo_4O_{11}.

The Magnéli phase Mo_4O_{11} has two modifications, γ- and η-Mo_4O_{11}.[2] Both are two-dimensional (2D) metals at room temperature and exhibit a resistivity anomaly at low temperature (the phase transition temperature T_p = 100 and 109 K for γ- and η-Mo_4O_{11}, respectively).[3,4] Diffuse X-ray and electron scattering studies on η-Mo_4O_{11} show that the resistivity anomaly originates from a charge density wave (CDW),[4a] which leads to the satellite peaks centered at (0, 0.23b^*, 0). Although the CDW affects the resistivity anisotropically, Mo_4O_{11} retains its 2D metallic character

---

(1) (a) Université de Paris-Sud. The Laboratoire de Chimie Théorique is associated with the CNRS (UA 506) and is a member of ICMO and IPCM (Orsay, France). (b) North Carolina State University. (c) Laboratoire d'Etudes des Propriétés Electroniques des Solides.

(2) (a) Magnéli, A. *Acta Chem. Scand.* **1948**, *2*, 861. (b) Kihlborg, L. *Ark. Kemi* **1963**, *21*, 365. (c) Ghedira, M.; Vincent, H.; Marezio, M.; Marcus, J.; Fourcaudot, G. *J. Solid State Chem.* **1985**, *56*, 66. (d) Greenblatt, M. *Chem. Rev.* **1988**, *88*, 31. (e) Schlenker, C.; Dumas, J.; Escribe-Filippini, C.; Guyot, H.; Marcus, J.; Fourcaudot, C. *Philos. Mag. B* **1985**, *52*, 643.

(3) (a) Guyot, H.; Schlenker, C.; Fourcaudot, G.; Konaté, K. *Solid State Commun.* **1985**, *54*, 909. (b) Sato, M.; Nakao, K.; Hoshino, S. *J. Phys. C* **1984**, *17*, L817. (c) Schlenker, C.; Parkin, S. S. P.; Guyot, H. *J. Magn. Magn. Mater.* **1986**, *54-57*, 1313.

(4) (a) Guyot, H.; Schlenker, C.; Pouget, J. P.; Ayroles, R.; Roucau, C. *J. Phys. C* **1985**, *18*, 4427. (b) Guyot, H.; Escribe-Filippini, C.; Fourcaudot, G.; Konaté, K.; Schlenker, C. *J. Phys. C* **1983**, *16*, L1227. (c) Gruber, H.; Krautz, E.; Fritzer, H. P.; Gatterer, K.; Popitsch, A. *Phys. Status Solidi A* **1984**, *86*, 749.

0020-1669/89/1328-1466$01.50/0 © 1989 American Chemical Society

below T_p. These properties of Mo_4O_{11} are quite analogous to those found for the sodium and potassium molybdenum purple bronzes $A_{0.9}Mo_6O_{17}$ (A = Na, K),[5] which are 2D metals at room temperature, have resistivity anomalies associated with a CDW at 120 K, and remain 2D metallic after the CDW transition.

Recently, tight-binding band electronic structure calculations[6] based upon the extended Hückel method[7] have been employed to examine the origin of the resistivity anomalies in the pseudo-one-dimensional (1D) metals molybdenum blue bronzes, $A_{0.3}MoO_3$ (A = K, Rb, Tl),[8,9] and lithium molybdenum purple bronze, $Li_{0.9}Mo_6O_{17}$,[10,11] as well as the 2D metal potassium molybdenum bronze, $K_{0.9}Mo_6O_{17}$.[5,12] Similar calculations on molybdenum red bronzes show[13] that they are regular semiconductors that have band gaps as a consequence of their O–Mo···O bond alternations. In the present work, we carry out a tight-binding band electronic structure study on Mo_4O_{11} to gain some insight into how its physical properties described above are related to the crystal structure. The atomic parameters employed in our work are identical with those used in the studies of the molybdenum bronzes.[8,10,12,13] In the following we first describe how the crystal structure of Mo_4O_{11} is assembled from MoO_6 octahedra and MoO_4 tetrahedra, which allows us to find simplified layer structures that represent the structural essence of Mo_4O_{11}. Then we describe the t_{2g}-block bands calculated for those model layers and discuss the physical properties of Mo_4O_{11} in terms of the Fermi surfaces calculated for the partially filled t_{2g}-block bands. Finally we carry out an orbital interaction analysis for the bottom portion of the t_{2g}-block bands that give rise to the Fermi surfaces.

Crystal Structure

Both γ- and η-Mo_4O_{11} contain layers of composition Mo_6O_{22}, solely made up of MoO_6 octahedra. Such layers are linked via MoO_4 tetrahedra to form the three-dimensional (3D) structures of Mo_4O_{11}. The γ- and η-Mo_4O_{11} phases differ slightly only in the way the Mo_6O_{22} layers are joined by the MoO_4 tetrahedra.[2] The Mo_6O_{22} layer structure may be derived from the Mo_3O_{16} chain **1**, which is obtained from three MoO_6 octahedra upon sharing the axial oxygen atoms. Shown in **2** is a schematic representation of the Mo_6O_{22} layer constructed from the Mo_3O_{16} chains **1** with the (11)(12) condensation pattern: In a given pair of adjacent Mo_3O_{16} chains, the first MoO_6 octahedron of the chain is condensed with that of the other chain. For the next pair of adjacent Mo_3O_{16} chains, the first MoO_6 octahedron of one chain is condensed with the second MoO_6 octahedron of the other chain. Every two adjacent MoO_6 octahedra of **2**, joined by an equatorial oxygen atom, form a zigzag Mo_2O_{10} chain **3** along the crystallographic *b* axis (not shown in **2** for simplicity).

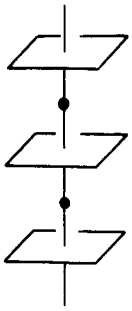

1

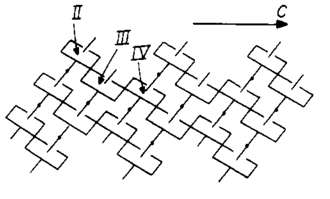

2

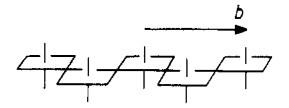

3

An MoO_6 octahedron of the Mo_6O_{22} layer **2** shares all six oxygen atoms with neighboring MoO_6 octahedra and/or MoO_4 tetrahedra. Thus, in **2**, an $Mo_{II}O_6$ octahedron is joined to three MoO_6 octahedra and three MoO_4 tetrahedra, an $Mo_{III}O_6$ octahedra to five MoO_6 octahedra and one MoO_4 tetrahedron, and an $Mo_{IV}O_6$ octahedron to six MoO_6 octahedra. The Zachariasen analysis[14] of the Mo–O bond lengths, in which the molybdenum oxidation state in the MoO_4 tetrahedral site is normalized to +6, shows that the Mo_{II}, Mo_{III}, and Mo_{IV} atoms have the oxidation states +5.8, +5.4, and +5.0, respectively.[2c] According to this analysis, d electrons of Mo_4O_{11} (i.e., two for formula unit Mo_4O_{11}) seem to reside in the $Mo_{III}O_6$ and $Mo_{IV}O_6$ octahedra.

Removal of the $Mo_{II}O_6$ octahedra from the Mo_6O_{22} layer **2** leads to the Mo_4O_{16} layer **4**. This layer can be regarded as obtained by the (11)(12) condensation of the Mo_2O_{11} chains **5**.

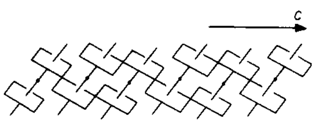

4

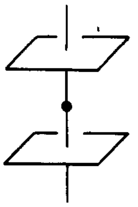

5

There are several important structural aspects to note from the

---

(5) (a) Buder, R.; Devenyi, J.; Dumas, J.; Marcus, J.; Mercier, J.; Schlenker, C. *J. Phys., Lett.* **1982**, *43*, L59. (b) Bervas, E.; Cochrane, R. W.; Dumas, J.; Escribe-Filippini, C.; Marcus, J.; Schlenker, C. *Lect. Notes Phys.* **1985**, 217. (c) Dumas, J.; Bervas, E.; Marcus, J.; Salomon, D.; Schlenker, C. *J. Magn. Magn. Mater.* **1983**, *31–34*, 535. (d) Escribe-Filippini, C.; Konate, K.; Marcus, J.; Schlenker, C.; Almairac, R.; Ayrolles, R.; Roucau, C. *Philos. Mag. B* **1984**, *50*, 321. (e) Greenblatt, M.; Ramanujachary, K. V.; McCarroll, W. H.; Neifeld, R.; Waszczak, J. V. *J. Solid State Chem.* **1985**, *59*, 149. (f) Gatehouse, B. M.; Lloyd, D. J.; Miskin, B. K. *NBS Spec. Publ.* (*U.S.*) **1972**, *No. 364*, 15. (g) Stephenson, N. C. *Acta Crystallogr.* **1966**, *20*, 59.

(6) Whangbo, M.-H.; Hoffmann, R. *J. Am. Chem. Soc.* **1978**, *100*, 6093.

(7) Hoffmann, R. *J. Chem. Phys.* **1963**, *39*, 1397.

(8) Whangbo, M.-H.; Schneemeyer, L. F. *Inorg. Chem.* **1986**, *25*, 2424.

(9) (a) Schlenker, C.; Dumas, J. In *Crystal Structures and Properties of Materials with Quasi One-Dimensional Structures*; Rouxel, J., Ed.; Reidel: Dordrecht, The Netherlands, 1986; p 135. (b) Wold, A.; Kunnmann, W.; Arnott, R. J.; Ferretti, A. *Inorg. Chem.* **1964**, *3*, 345. (c) Stephenson, N. C.; Wadsley, A. D. *Acta Crystallogr.* **1965**, *18*, 241. (d) Bouchard, G. H.; Perlstein, J. H.; Sienko, M. J. *Inorg. Chem.* **1967**, *6*, 1682. (e) Pouget, J. P.; Noguera, C.; Moudden, A. H.; Moret, T. *J. Phys.* (*Les Ulis, Fr.*) **1985**, *46*, 1731. (f) Pouget, J. P.; Kagoshima, S.; Schlenker, C.; Marcus, J. *J. Phys., Lett.* **1983**, *44*, L113. (g) Fleming, R. M.; Schneemeyer, L. F.; Moncton, D. E. *Phys. Rev. B: Condens. Matter* **1985**, *31*, 899. (h) Sato, M.; Fujishita, H.; Hoshino, S. *J. Phys. C* **1985**, *18*, 2603.

(10) Whangbo, M.-H.; Canadell, E. *J. Am. Chem. Soc.* **1988**, *110*, 358.

(11) (a) Onoda, M.; Toriumi, K.; Matsuda, Y.; Sato, M. *J. Solid State Chem.* **1987**, *66*, 163. (b) Schlenker, C.; Schwenk, H.; Escribe-Filippini, C.; Marcus, J. *Physica B+C* **1985**, *135B+C*, 511. (c) Greenblatt, M.; McCarroll, W. H.; Neifeld, R.; Croft, M.; Waszczak, J. V. *Solid State Commun.* **1984**, *51*, 671. (d) Ramanujachari, K. V.; Collins, B. T.; Greenblatt, M.; McNally, P.; McCarroll, W. H. *Solid State Ionics* **1986**, *22*, 105. (e) Matsuda, Y.; Onoda, M.; Sato, M. *Physica B+C* **1986**, *143B+C*, 243.

(12) Whangbo, M.-H.; Canadell, E.; Schlenker, C. *J. Am. Chem. Soc.* **1987**, *109*, 6308.

(13) (a) Canadell, E.; Whangbo, M.-H. *Inorg. Chem.* **1988**, *27*, 228. (b) Whangbo, M.-H.; Evain, M.; Canadell, E.; Ganne, M. *Inorg. Chem.* 1989, *28*, 267.

(14) Zachariasen, W. H. *J. Less-Common Met.* **1978** *62*, 1.

Mo_4O_{16} layer **4**: (a) Along the crystallographic *b* axis, the layer **4** consists of the Mo_4O_{18} chains **6**. These chains are important

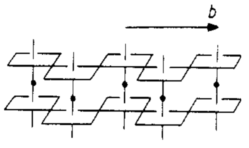

6

building blocks of lithium molybdenum purple bronze, $Li_{0.9}Mo_6O_{17}$.[10] (b) As schematically shown by the perspective view **7**, the Mo_4O_{16} layer **4** is a stepped layer. (c) The stepped layer

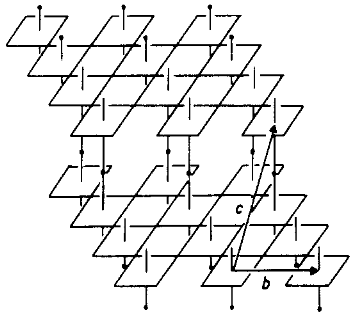

7

7 (i.e., **4**) is constructed either from the Mo_4O_{18} chains **6** or from the Mo_4O_{21} chains **8** by appropriate axial and/or equatorial corner sharings.

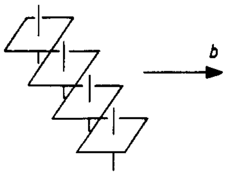

8

Band Electronic Structure

The low-lying part of the d-block bands of Mo_4O_{11} is represented by the t_{2g}-block bands of the Mo_6O_{22} layers **2**. Furthermore, only the bottom portion of those t_{2g}-block bands is filled because Mo_4O_{11} has two d electrons per formula unit (or, equivalently, four d electrons per repeat unit of the Mo_6O_{22} layer **2**). Thus, in interpreting the electrical properties of γ- and η-Mo_4O_{11}, it is sufficient to examine the t_{2g}-block bands of the Mo_6O_{22} layer **2** found in Mo_4O_{11}. To help understand the nature of those bands, we also examine the t_{2g}-block bands calculated for the ideal and real structures of Mo_4O_{18} chain **6**. W construct the ideal chain and layer structures with regular MoO_6 octahedra having Mo–O = 1.945 Å (i.e., the average of the various Mo–O distances of the MoO_6 octahedra found in Mo_4O_{11}).

Figure 1 shows the t_{2g}-block bands calculated for the ideal Mo_4O_{18} chain **6**, which has four dispersive and eight flat bands. A detailed description of those bands was given elsewhere in connection with $Li_{0.9}Mo_6O_{17}$.[10] Figure 2 shows the t_{2g}-block bands calculated for the ideal Mo_4O_{16} layer **4**. The four bands a, b, c, and d are dispersive only along $\Gamma \rightarrow Y$ (i.e., along the Mo_4O_{18} chain direction) and have 1D-like character. These bands are related in orbital nature to the four dispersive bands of the Mo_4O_{18} chain **6** shown in Figure 1. The four bands e, f, g, and h of Figure 2 are each practically doubly degenerate. The bands e, f, and h are dispersive along both $\Gamma \rightarrow Y$ and $\Gamma \rightarrow Z$ directions and thus have 2D-like character. These bands are related in nature to the eight flat bands of the Mo_4O_{18} chain shown in Figure 1. The dispersive nature of these three bands e, f, and h stems from the interactions between the Mo_4O_{18} chains **6** through their bridging-axial oxygen atoms in the Mo_4O_{16} layer (see **7**).

Figure 3 shows the t_{2g}-block bands calculated for the real Mo_4O_{16} layer **4**, taken from the crystal structure of γ-Mo_4O_{11}.[2c] With respect to the ideal Mo_4O_{16} layer, the real Mo_4O_{16} layer shows degeneracy lifting and band noncrossings in its t_{2g}-block bands due to the lowering of symmetry (i.e., irregular MoO_6 octahedra in the real Mo_4O_{16} layer). Except for these minor modifications, the t_{2g}-block bands of the ideal and real Mo_4O_{16} layers are essentially identical. In particular, the bottom three bands of Figure 3 are only slightly different from those of Figure 2.

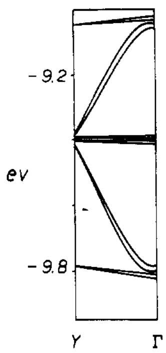

Figure 1. Dispersion relations of the t_{2g}-block bands calculated for the ideal Mo_4O_{18} chain **6**, where $\Gamma = 0$ and $Y = b^*/2$.

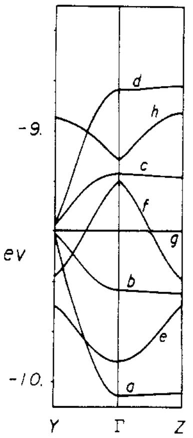

Figure 2. Dispersion relations of the t_{2g}-block bands calculated for the ideal Mo_4O_{16} layer **4** (i.e., **7**), where $\Gamma = (0, 0)$, $Y = (b^*/2, 0)$, and $Z = (0, c^*/2)$.

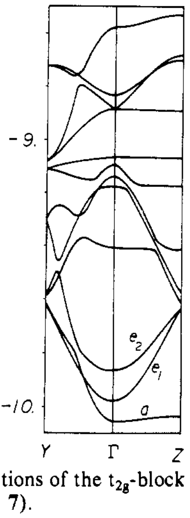

Figure 3. Dispersion relations of the t_{2g}-block bands calculated for the real Mo_4O_{16} layer **4** (i.e., **7**).

Shown in Figure 4 is the bottom portion of the t_{2g}-block bands calculated for the real Mo_6O_{22} layer **2**, taken from the crystal structure of γ-Mo_4O_{11}.[2c] With four d electrons to fill these bands, the Fermi level (shown by the dashed line) cuts the bottom three bands a, e_1, and e_2. Along $\Gamma \rightarrow Y$ and $\Gamma \rightarrow Z$ these partially filled bands are essentially identical with the bottom three bands of Figure 3, except that the band e_1 is slightly lower in energy in the real Mo_6O_{22} layer. Therefore, as shown in the next section, the essential features of the band structure of the Mo_6O_{22} layer

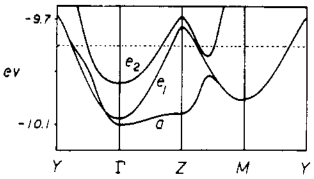

Figure 4. Dispersion relations of the t_{2g}-block bands calculated for the real Mo_6O_{22} layer **2**, where $M = (b^*/2, c^*/2)$ and the dashed line refers to the Fermi level.

Table I. Antibonding Contributions of the Oxygen p Orbitals of Mo–O–Mo Bridges in the Lower t_{2g}-Block Band Orbitals of the Mo_4O_{16} Layer[a]

			bridging O		
				between nearest-neighbor unit cells	
band	wave vector	step orbital	within a unit cell	eq	ax
a	Γ	**17**	NNN	NNN	NN
	Y	**18**	NNN	YYY	NN
	Z	**17**	NNN	NNN	NN
b	Γ	**19**	NYN	NYN	NN
	Y	**20**	NYN	YNY	NN
	Z	**19**	NYN	NYN	NN
e	Γ	**22**	NNN	NNN	NN
	Y	**23**	NNN	NNN	YY
	Z	**22**	NNN	NNN	YY

[a] The presence of a stronger or weaker antibonding contribution is indicated by the symbol Y or y, respectively, and the absence of it by the symbol N.

2 (and hence those of Mo_4O_{11}) can be understood by simply analyzing the band structure of the Mo_4O_{16} layer **4**. The band dispersions of Figure 4 along $Z \rightarrow M$ show that the 1D-like band a interacts with one of the two 2D-like bands to give rise to the band noncrossing along $Z \rightarrow M$.

Orbital Nature of the t_{2g}-Block Bands

The electrical and other physical properties of the Magnêli phase Mo_4O_{11} are primarily governed by the bottom three t_{2g}-block bands of the Mo_6O_{22} layer **2**, which are partially filled. Since these three bands are almost identical with those of the Mo_4O_{16} layer (see Figures 3 and 4), we now probe the orbital character of those bands on the basis of the bands a, b, and e calculated for the ideal Mo_4O_{16} layer.

Interaction Patterns. As can be seen from the perspective view **7**, the Mo_4O_{16} layer is constructed from the Mo_4O_{21} chains **8** by sharing three equatorial oxygen atoms along the b axis and by sharing two axial oxygen atoms between "steps". In the crystal structures made up of corner-sharing MoO_6 octahedra, the metal d orbitals overlap primarily with the p orbitals of its adjacent oxygen atoms. Thus, the dispersion relations of the d-block bands of such compounds are easily deduced by simply determining[8,10,12,15] whether or not the bridging oxygen p orbitals can mix with the metal d orbitals at high-symmetry wave vector points such as Γ, Y, and Z.

The three t_{2g}-block d orbitals of an ideal MoO_6 octahedron are shown in **9**, where the orbitals of the surrounding oxygen atoms make antibonding contributions to the metal atom (not shown for simplicity). Orbital combination patterns around a bridging-equatorial oxygen atom are shown in **10**–**12**, while those around a bridging-axial oxygen atom are shown in **13**–**15**. In **10**–**14** the bridging atom p orbital is antibonding with the two adjacent metal d orbitals when the latter are in phase. Out-of-phase combinations of two adjacent metal d orbitals do not allow the mixing of a bridging atom p orbital. As shown in **15**, the axial oxygen atom cannot combine with the δ orbitals regardless of their relative phases.

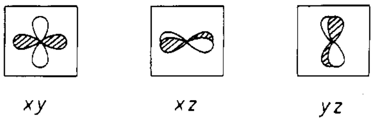

9

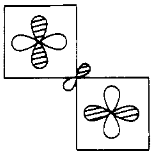

10a

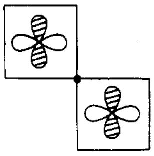

10b

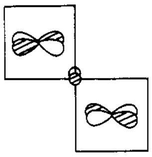

11a

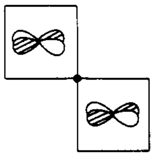

11b

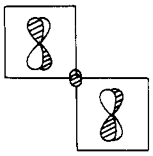

12a

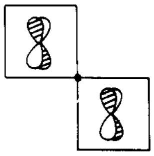

12b

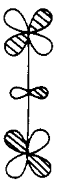

13a

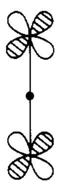

13b

14a

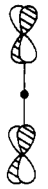

14b

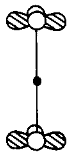

15a

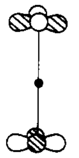

15b

The extent of the antibonding between the metal and the bridging atoms is stronger in **10a**, **14a**, and **13a** than in **11a** and **12a**, because the all-planar arrangement of the orbitals provides a more effective overlap and hence a greater antibonding.[10,12] In our discussion, the presence of a bridging oxygen p orbital in band orbitals is denoted by the symbol Y for the stronger antibonding as in **10a**, **14a**, or **13a** and by the symbol y for the weaker antibonding as in **11a** or **12a**. The absence of a bridging oxygen p orbital in band orbitals is denoted by the symbol N. In general, one Y interaction is approximately equal in magnitude to two y interactions.[10,12]

δ Band. The band a of Figure 2 is constructed from the orbital **16a** of the Mo_4O_{21} unit **8** (i.e., the lowest lying δ orbital of the

---

(15) Whangbo, M.-H. In *Crystal Structures and Properties of Materials with Quasi One-Dimensional Structures*; Rouxel, J., Ed.; Reidel: Dordrecht, The Netherlands, 1986; p 27.

unit). Within this unit, the three equatorial-bridging oxygen atoms have no contributions to **16a**; i.e., they have the NNN contribution to **16a**. The band a at Γ and that at *Y* are given by the "step" orbitals **17** and **18**, respectively, which show the orbitals for one step of the Mo_4O_{16} layer (see **8**). Between the Mo_4O_{21} units along the *b* axis, the three equatorial bridging atoms have the NNN and YYY contributions to **17** and **18**, respectively. Thus band a is less stable at *Y* at Γ by three Y interactions per Mo_4O_{21} unit. The step orbital of band a at *Z* is also given by **17**. Along the *c* axis, the step orbitals **17** combine in phase at Γ but out of phase at *Z*. The two bridging-axial atoms of each Mo_4O_{21} unit have the NN contribution to these band orbitals, due to the δ symmetry of the metal d orbitals. Therefore, band a is dispersive along Γ → *Y* and remains flat along Γ → *Z*.

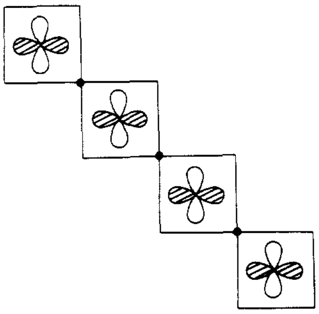

16a

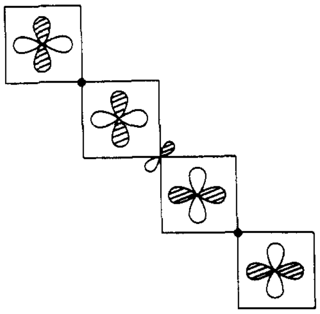

16b

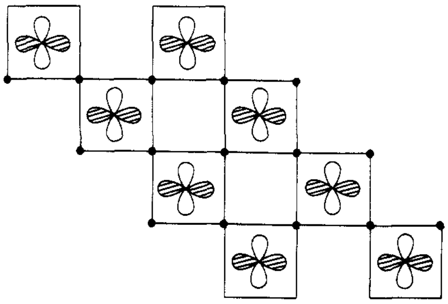

17

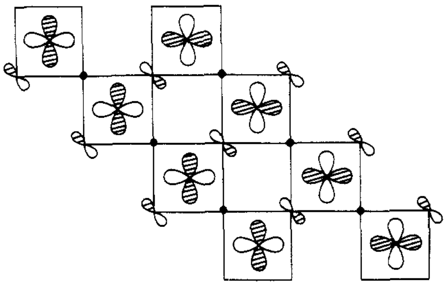

18

Band b of Figure 2 is constructed from orbital b of the Mo_4O_{21} unit (i.e., the second lowest lying δ orbital of the unit). Within this unit, **16b** has the NYN contribution from the three bridging equatorial oxygen atoms. Band b at Γ and *Y* has the step orbitals **19** and **20**, respectively. Between the Mo_4O_{21} units along the *b* axis, **19** and **20** have the NYN and YNY contributions from the bridging-equatorial oxygen atoms, respectively. Therefore, **19** and **20** are less stable than **17** by two and three Y interactions per Mo_4O_{21} unit, respectively. Thus, with respect to band a, band b lies higher in energy and is less dispersive along Γ → *Y*. Band b is flat along Γ → *Z* for the same reason band a is flat along Γ → *Z*. Table I lists the contributions of the bridging-oxygen p orbitals to bands a, b, and e at Γ, *Y*, and *Z*.

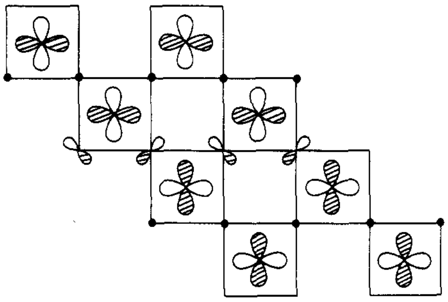

19

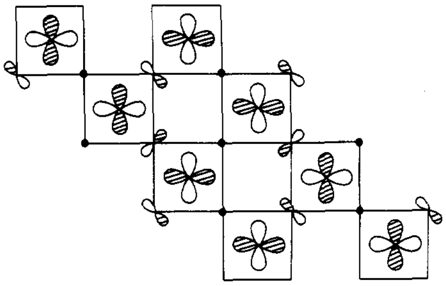

20

π Band. The doubly degenerate band e of Figure 2 is constructed from the orbitals **21a** and **21b**. Both are the lowest lying π orbitals of the Mo_4O_{21} unit **8**. Within this unit, the three bridging-equatorial oxygen atoms have the NNN contribution to **21a** and **21b**. One of the two degenerate bands e has the step orbitals **22** and **23** at Γ and *Y*, respectively. Between the Mo_4O_{21} units, **22** and **23** have the NNN contribution from the three

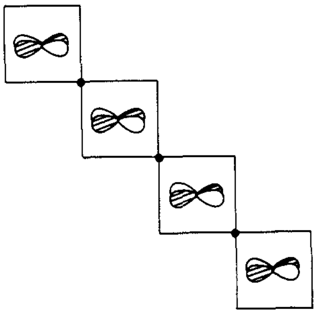

21a

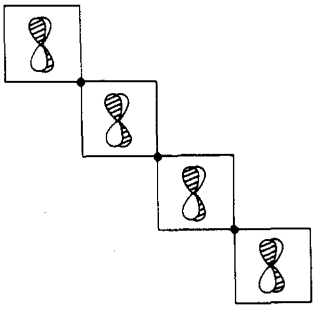

21b

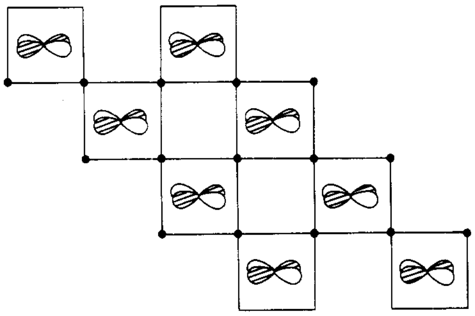

22

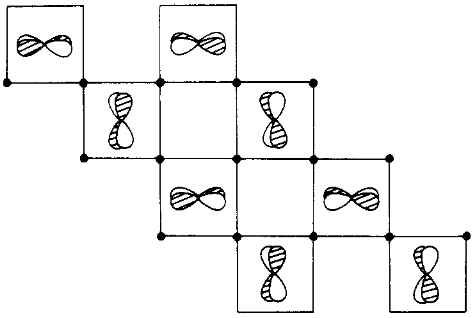

23

bridging-equatorial oxygen atoms. At Γ and Y the step orbitals repeat with the same sign along the c axis, so that **22** and **23** have the NN and YY contributions, respectively, from the two bridging-axial oxygen atoms per Mo_4O_{21} unit. At Z, however, the step orbitals **22** repeat with alternating signs along the c axis. Thus, band orbital e at Z has the YY contribution from the two bridging-axial oxygen atoms per Mo_4O_{21} unit. Therefore, as listed in Table I, band e goes up in energy along both $\Gamma \rightarrow Y$ and $\Gamma \rightarrow Z$. That is, band e is 2D-like. The same conclusion is obtained for the other of the two degenerate bands e.

Band Filling and Dimensionality. According only to the bridging oxygen contributions listed in Table I, the 2D-like band e at Γ and the 1D-like band a at Γ would have the same energy. However, one must take into consideration the antibonding contributions from the eight nonbridging oxygen atoms of each Mo_4O_{21} unit (i.e., four axial and four equatorial oxygen atoms in **8**). The p orbitals of the nonbridging axial oxygen atoms do not combine with the metal δ orbitals, but they do with the metal π orbitals. Consequently, at Γ, band e (derived from the metal π orbitals) lies slightly higher in energy than band a (derived from the metal δ orbitals).

A striking feature of the bottom two bands a and e of the ideal Mo_4O_{16} layer (and hence the bottom three bands a, e_1, and e_2 of the real Mo_4O_{16} or Mo_6O_{22} layer) is that they have nearly the same energy at Γ, which is due to the fact that their band orbitals do not have p-orbital contributions from the bridging oxygen atoms. Thus, the bottom three bands a, e_1, and e_2 of the real Mo_6O_{22} layer overlap significantly. With four d electrons to fill the a, e_1, and e_2 bands, it is therefore unlikely that the 1D-like band a will be either one-fourth or three-fourths filled even if the interaction between the 1D-like band a and the 2D-like band e_2 (e.g., along $Z \rightarrow M$ in Figure 4) can be completely removed so as to make them effectively cross each other. This is important in our discussion of the origin of the electronic instability in Mo_4O_{11} in the next section.

Fermi Surfaces and CDW

The Mo_6O_{22} layer **2** has the bottom three of its t_{2g}-block bands partially filled. The Fermi surfaces associated with those bands a, e_1, and e_2 are shown in parts a–c of Figure 5, respectively. Since bands a and e_1 merge into a single band (along $Z \rightarrow M \rightarrow Y$ of Figure 4), their Fermi surfaces should be combined into one in the extended zone scheme as illustrated in Figure 6a. Thus, the Mo_6O_{22} layer, and therefore Mo_4O_{11}, has the hole pockets given by Figure 6a and the electron pockets given by Figure 5c. All those Fermi surfaces are closed so that Mo_4O_{11} is predicted to be a 2D metal, as experimentally observed.[3,4]

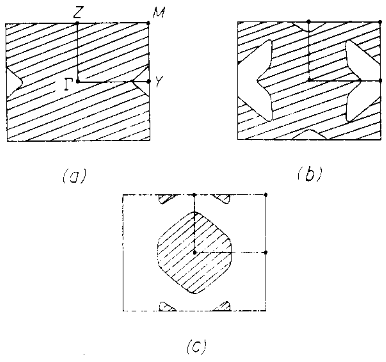

Figure 5. Fermi surfaces associated with the partially filled bands (a) a, (b) e_1, and (c) e_2 of the Mo_6O_{22} layer **2**. The wave vectors of the shaded and unshaded regions refer to filled and unfilled band levels, respectively.

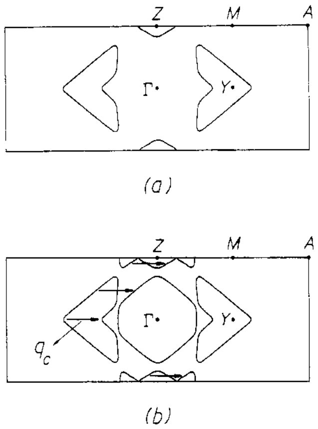

Figure 6. (a) Combined hole Fermi surface in the extended zone scheme for bands a and e_1 of the layer **2**, where $A = (b^*, c^*/2)$. (b) Combined electron and hole surfaces in the extended zone scheme, where the nesting vector is given by $\mathbf{q}_c \simeq (0.25b^*, 0)$.

The hole Fermi surfaces of Figure 6a and the electron Fermi surfaces of Figure 5c are combined together in Figure 6b. In each heart-shaped hole surface, the "V-shaped" portions are related to each other by the translation $\mathbf{q}_c \simeq (0.25b^*, 0)$; i.e., they are nested by $\mathbf{q}_c$. The remaining portions of the hole surfaces, except for those parallel to the $\Gamma \rightarrow Z$ direction, are found to be nested to the appropriate portions of the electron surfaces by $\mathbf{q}_c$ as indicated by the arrows. This nesting might be responsible for the superlattice spots at $(0, 0.23b^*, 0)$ observed for η-Mo_4O_{11} below T_p.[4a] The occurrence of such superlattice spots typically implies the presence of a nearly one-fourth- or three-fourths-filled 1D band.[15,16] It is interesting to argue that band a of Figure 4 becomes purely 1D in character at T_p upon removing its interaction with band e_2. However, the resulting 1D band cannot be either one-fourth or three-fourths filled, as discussed in the previous section. Thus, the nesting given by the vector $\mathbf{q}_c$ in Figure 6b is the most likely reason for the electronic instability associated with the superlattice spots at $(0, 0.23b^*, 0)$. Since the nesting given by $\mathbf{q}_c$ is not complete, the electron and hole surfaces would not be completely removed by the CDW associated with $\mathbf{q}_c$. This expectation is consistent with the observation that Mo_4O_{11} remains metallic below T_p.

Concluding Remarks

The Magnéli phases γ- and η-Mo_4O_{11} are 2D metals but exhibit a resistivity anomaly at low temperature. These two phases differ slightly in how their building blocks, Mo_6O_{22} layers made up of MoO_6 octahedra, are linked by MoO_4 tetrahedra. Mo_4O_{11} has

---

(16) Moret, R.; Pouget, J. P. In *Crystal Structures and Properties of Materials with Quasi One-Dimensional Structures*; Rouxel, J., Ed.; Reidel: Dordrecht, The Netherlands, 1986; p 87.

two d electrons per formula unit, and these electrons are primarily confined in the Mo_6O_{22} layers. Thus, only the bottom three of the t_{2g}-block bands of the Mo_6O_{22} layer are partially filled. Our orbital interaction analysis shows that the three partially filled bands are close in energy at Γ, because this wave vector prevents the bridging oxygen p orbitals from mixing with the metal d orbitals. The Fermi surfaces associated with the partially filled bands are all closed, in agreement with the observation that Mo_4O_{11} is a 2D metal. However, the Fermi surfaces show a partial nesting, which is consistent with the superlattice spots at $(0, 0.23b^*, 0)$ found for η-Mo_4O_{11}. The resistivity anomaly in γ- and η-Mo_4O_{11} is most likely to originate from a CDW associated with this partial nesting.

Acknowledgment. M.-H.W. and E.C. thank Dr. J. P. Pouget for invaluable discussions concerning the Fermi surfaces of Mo_4O_{11}. This work was supported by NATO, Scientific Affairs Division, and also by DOE, Office of Basic Sciences, Division of Materials Science, under Grant DE-FG05-86ER45259.

Registry No. Mo_4O_{11}, 12033-38-4.

Contribution from The Frank J. Seiler Research Laboratory,
U.S. Air Force Academy, Colorado Springs, Colorado 80840

Calculation of Hydrogen-Bonding Interactions between Ions in Room-Temperature Molten Salts

Chester J. Dymek, Jr.,* and James J. P. Stewart

Received April 26, 1988

The nature of the interactions between the ions in room-temperature molten salts formed by mixing $AlCl_3$ with 1-methyl-3-ethylimidazolium chloride ((MEI)Cl) is of interest because of its relevance to the transport and electrochemical properties of these melts. The results of AM1 semiempirical molecular orbital calculations using the MOPAC program support the interpretation of experimental results in which MEI^+ is hydrogen-bonded to Cl^- ions at the 2-, 4-, and 5-carbons of the MEI^+ ring. A new approach to the characterization of vibrational modes calculated in MOPAC is introduced to more clearly relate the calculated vibrations in the proposed model to experimental results.

Mixtures of 1-methyl-3-ethylimidazolium chloride ((MEI)Cl) and $AlCl_3$ form chloroaluminate salts that are liquid well below room temperature.[1] These melts are of interest as electrolytes, as nonaqueous solvents for studying ionic complexes, and as catalytic solvents for Friedel–Crafts reactions.[2]

The main reactions that occur in the formation of the melts and that explain their interesting acid–base behavior are given as follows:

$$MEI^+Cl + AlCl_3 \rightarrow MEI^+AlCl_4^- \quad K \gg 1$$

$$MEI^+AlCl_4^- + AlCl_3 \rightarrow MEI^+Al_2Cl_7^- \quad K \gg 1$$

Melts formed with mole fraction N of $AlCl_3$ less than 0.5 will have $AlCl_4^-$ and Cl^-, a Lewis base, present and are thus basic melts. Those with $N > 0.5$ contain $AlCl_4^-$ and $Al_2Cl_7^-$, a Lewis acid, and are thus acidic melts. The structure of MEI^+ with ring carbons numbered is shown as follows:

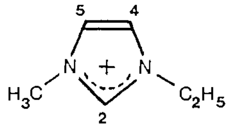

MEI^+

An important aspect of the melts that needs to be further understood is the nature of the interactions among the ions present. The questions of particular interest are the following. Is there ion-pair formation in the melt? Are there specific points on the MEI^+ at which interactions with counterions, particularly Cl^-, occur? Can the transport properties of the melts be understood in terms of these interactions?

NMR[3] and IR[4,5] studies on $(MEI)Cl/AlCl_3$ melts and crystallographic studies[6] of solid (MEI)Cl have been used to propose models for the ionic interactions in the melt. The main differentiation in the models is whether hydrogen bonding occurs between the Cl^- ions and the ring carbons of MEI^+. In a study that presented evidence against hydrogen bonding to Cl^- solely at the C2 hydrogen of MEI^+,[5] a stack model of melt ionic interactions was proposed to explain IR spectral evidence that showed that all three C–H stretches were affected by the presence of Cl^- in basic melts. In this model a Cl^- was sandwiched between two parallel MEI^+ ions that in turn had $AlCl_4^-$ ions on their outer sides. Semiempirical molecular orbital calculations predicted this stack cluster to be stable when fully optimized with the Cl^- approximately centered between the C2's of the two parallel MEI^+ rings. Uncertainty in the validity of this model stemmed from its failure to predict the shift to lower frequencies and the increase in intensity of the C–H stretches experimentally observed with addition of Cl^-. In fact, the ring C–H stretch frequencies differed only slightly from those calculated for an isolated MEI^+. However, attempts to calculate a stable optimized system in which Cl^- is hydrogen-bonded to MEI^+ through the ring C2–H bond also failed. The Cl^- either bonded covalently to C2 of the ring or, if constrained to line up along the C2–H bond, formed virtually a covalent bond with the H. It was acknowledged that these results could not be used to rule out hydrogen bonding of Cl^- to MEI^+ because of the known exaggeration of the instability of Cl^- in the computational method used.

In this work we used the MOPAC program[7] to calculate the optimized molecular structure of MEI^+ in varying ionic environments and then the IR spectra of these optimized systems. We then compared our results with experimental evidence to arrive at a description of the dominant features of the interaction of MEI^+ with Cl^- ions in basic melts.

Computational Methods

The MOPAC program, which incorporates the MNDO,[8] AM1,[9] and MINDO/3[10] semiempirical molecular orbital methods originally developed by Dewar and co-workers, has been applied with some success to

---

(1) Fannin, A. A., Jr.; Floreani, D. A.; King, L. A.; Landers, J. S.; Piersma, B. J.; Stech, D. J.; Vaughn, R. L.; Wilkes, J. S.; Williams, J. L. *J. Phys. Chem.* **1984**, *88*, 2614.

(2) Hussey, C. L. *Advances in Molten Salt Chemistry*; Mamantov, G., Mamantov, C., Eds.; Elsevier: New York, 1983; Vol. 15, p 185.

(3) Fannin, A. A., Jr.; King, L. A.; Levisky, J. A.; Wilkes, J. S. *J. Phys. Chem.* **1984**, *88*, 2609.

(4) Tait, S.; Osteryoung, R. A. *Inorg. Chem.* **1984**, *23*, 4352.

(5) Dieter, K. M.; Dymek, C. J., Jr.; Heimer, N. D.; Rovang, J. W.; Wilkes, J. S. *J. Am. Chem. Soc.* **1988**, *110*, 2722.

(6) Dymek, C. J., Jr.; Fratini, A. V.; Adams, W. W.; Grossie, D. A. *Inorg. Chem.*, in press.

(7) Stewart, J. J. P. *Quantum Chem. Prog. Exchange Bull.* **1987**, *7(4)*, addendum.

(8) Dewar, M. J. S.; Thiel, W. *J. Am. Chem. Soc.* **1977**, *99*, 4899.

(9) Dewar, M. J. S.; Zoebisch, E. G.; Healy, E. F.; Stewart, J. J. P. *J. Am. Chem. Soc.* **1985**, *107*, 392.

(10) Bingham, R. C.; Dewar, M. J. S.; Lo, D. H. *J. Am. Chem. Soc.* **1975**, *97*, 1285.